Supplemental Material for Renormalization of networks with weak geometric coupling

Jasper van der Kolk,[1,2,*] Marián Boguñá,[1,2,†] and M. Ángeles Serrano[1,2,3,‡]

[1] *Departament de Física de la Matèria Condensada, Universitat de Barcelona, Martí i Franquès 1, E-08028 Barcelona, Spain*
[2] *Universitat de Barcelona Institute of Complex Systems (UBICS), Barcelona, Spain*
[3] *Institució Catalana de Recerca i Estudis Avançats (ICREA), Passeig Lluís Companys 23, E-08010 Barcelona, Spain*

CONTENTS

S1. SELF-SIMILARITY OF THE CONNECTION PROBABILITY

In this section we show that the connection probability

$$p_{ij} = \left(1 + \frac{(R\Delta\theta_{ij})^{\beta}}{(\hat{\mu}\kappa_i\kappa_j)^{\max(1,\beta)}}\right)^{-1} \tag{S1}$$

is self-similar under renormalization if certain choices are made. In the renormalization procedure described above, supernodes in layer $l+1$ are formed by combining r adjacent nodes from layer l. If any constituent of supernode σ, denoted by the set $\mathcal{S}(\sigma)$ is connected to any of the constituents of supernode τ they are said to be connected. The probability of this being the case is given by

$$p_{\sigma\tau}^{(l+1)} = 1 - \prod_{(i,j)\in\mathcal{P}(\sigma,\tau)} (1 - p_{ij}^{(l)}), \tag{S2}$$

i.e. one minus the probability that none of the constituents are connected. Here we have defined $\mathcal{P}(\sigma,\tau) = S(\sigma)\times S(\tau)$. Using that $p_{ij}^{(l)} = 1/(1-x_{ij}^{(l)})$ we can rewrite this expression as

$$p_{\sigma\tau}^{(l+1)} = 1 - \frac{1}{\prod_{(i,j)\in\mathcal{P}(\sigma,\tau)}(1 + (x_{ij}^{(l)})^{-1})}. \tag{S3}$$

The denominator of the second term can be expanded as

$$\prod_{(i,j)\in\mathcal{P}(\sigma,\tau)} (1 + (x_{ij}^{(l)})^{-1}) = 1 + \sum_{(i,j)\in\mathcal{P}(\sigma,\tau)} (x_{ij}^{(l)})^{-1} + \sum_{(i,j)\in\mathcal{P}(\sigma,\tau)} (x_{ij}^{(l)})^{-1} \sum_{(s,t)\in\mathcal{P}(\sigma,\tau)\setminus(n,m)} (x_{st}^{(l)})^{-1} + ... \tag{S4}$$

* jasper.vanderkolk@ub.edu
† marian.boguna@ub.edu
‡ marian.serrano@ub.edu

We know that $x_{ij}^{(l)} = (R^{(l)}\Delta\theta_{ij}^{(l)})^{\beta^{(l)}}/(\hat{\mu}^{(l)}\kappa_i^{(l)}\kappa_j^{(l)})^{\max(1,\beta^{(l)})}$ which is proportional to $(N^{(l)})^{\max(1,\beta^{(l)})} \gg 1$. Thus, we can truncate the expansion at first order. We assume that $\Delta\theta_{ij}^{(l)} \approx \Delta\theta_{\sigma\tau}^{(l+1)}$, the distance between the two supernodes. This is because the distances between the nodes within a single supernode is generally much smaller than the distance between nodes in different supernodes. This allows us to rewrite Eq. (S3) as

$$p_{\sigma\tau}^{(l+1)} = \left(1 + \frac{\left(R^{(l)}\Delta\theta_{\sigma\tau}^{(l+1)}\right)^{\beta^{(l)}}}{\sum_{(i,j)\in\mathcal{P}(\sigma,\tau)}\left(\hat{\mu}^{(l)}\kappa_i^{(l)}\kappa_j^{(l)}\right)^{\max(1,\beta^{(l)})}}\right)^{-1}. \tag{S5}$$

In order for this to be a proper connection probability in the renormalized layer, taking into account that $R^{(l+1)} = R^{(l)}/r$ and $\beta^{(l+1)} = \beta^{(l)} \equiv \beta$, we must demand $\hat{\mu}^{(l+1)} = \hat{\mu}^{(l)}/r^{\min(1,\beta)}$. Furthermore, the evolution of the hidden degrees is as follows

$$\kappa_\sigma^{(l+1)} = \left(\sum_{i\in\mathcal{S}(\sigma)}\left(\kappa_i^{(l)}\right)^{\max(1,\beta)}\right)^{1/\max(1,\beta)}. \tag{S6}$$

This transformation respects the semi-group property of the renormalization as

$$\begin{aligned}\kappa_\sigma^{(l+2)} &= \left(\sum_{i\in\mathcal{S}(\sigma)}(\kappa_i^{(l+1)})^{\max(1,\beta)}\right)^{1/\max(1,\beta)} \\ &= \left(\sum_{i\in\mathcal{S}(\sigma)}\sum_{s\in\mathcal{S}(i)}(\kappa_s^{(l)})^{\max(1,\beta)}\right)^{1/\max(1,\beta)}.\end{aligned} \tag{S7}$$

This final double sum is equivalent to a single sum over all r^2 nodes in the unrenormalized layer l that make up the supernode in the layer $l+2$.

In the similarity dimension we have slightly more freedom, as we just need to find a definition of $\Delta\theta_{\sigma\beta}^{(l+1)}$ that (1) respects the semi-group property of the renormalization procedure, (2) respects the spherical symmetry of the system and (3) lies in the range defined by the angular coordinates of the constituent nodes and therefore respects the original node order. We therefore define

$$\theta_\sigma^{(l+1)} = \frac{\sum_{i\in S(\sigma)}(\kappa_i^{(l)})^{\max(1,\beta)}\theta_i^{(l)}}{\sum_{i\in S(\sigma)}(\kappa_i^{(l)})^{\max(1,\beta)}}, \tag{S8}$$

which can been seen as a weighted average. Note that we do not choose the exact definition as given in Ref. [1] because it introduces a bias for the constituent node with the largest angular coordinate when $\beta > 1$.

The definition in Eq. (S8) works well as long as the difference between the largest and smallest coordinate is smaller than π, but breaks down when this is not the case. If, for example, we try and create a supernode from the coordinates $(\kappa_1^{(l)}, \theta_1^{(l)}) = (1, \pi/4)$ and $(\kappa_2^{(l)}, \theta_2^{(l)}) = (1, 7\pi/4)$, we end up with $(\kappa^{(l+1)}, \theta^{(l+1)}) = (2^{1/\max(1,\beta)}, \pi)$. This obviously is not correct, as the supernode lies on the opposite side of the unit circle from where its constituents were located. As we normally define supernodes by taking adjacent constituent nodes, starting from the node with the smallest angular coordinate, we do not run into this problem. However, in the main text we compare the ordered renormalization with one where the constituent nodes are chosen at random, and thus Eq. (S8) can in principle not be applied. Note that in this case also the argument used to obtain Eq. (S5) fails, and so we cannot expect the connection probability in the renormalized layer to be congruent with the $\mathbb{S}^1$ model when the angular coordinate is relevant. The generalization of the renormalized angular coordinate is given by

$$\theta_\sigma^{(l+1)} = \arg\left(\frac{\sum_{i\in S(\sigma)}(\kappa_i^{(l)})^{\max(1,\beta)}e^{\mathrm{i}\theta_i^{(l)}}}{\sum_{i\in S(\sigma)}(\kappa_i^{(l)})^{\max(1,\beta)}}\right), \tag{S9}$$

which can be seen as a weighted circular mean.

When the spread of the constituent angular coordinates is small, as is the case for GR, it does not matter which of the two definitions of $\theta_\sigma^{(l+1)}$ one takes: Let $\{\theta_1^{(l)},...,\theta_r^{(l)}\}$ be the set of constituent nodes of a supernode σ in layer $l+1$, sorted in ascending order and where we assume that $\theta_r^{(l)}-\theta_1^{(l)} \ll 1$. Then we know that $\Delta\theta_{i1}^{(l)} \ll 1\ \forall i$, which allows us to approximate Eq. (S9) as

$$\begin{aligned}\theta_\sigma^{(l+1)} &\approx \arg\left(\frac{e^{i\theta_1^{(l)}}\sum_{i\in\mathcal{S}(\sigma)}\kappa_i^{\max(1,\beta)}\left(1+\mathrm{i}\Delta\theta_{i1}^{(l)}\right)}{\sum_{i\in S(\sigma)}\kappa_i^{\max(1,\beta)}}\right)\\ &= \arg\left(e^{\mathrm{i}\theta_1^{(l)}}\left(1+\mathrm{i}\overline{\Delta\theta^{(l)}}\right)\right) \approx \arg\left(e^{\mathrm{i}\theta_1^{(l)}}e^{\mathrm{i}\overline{\Delta\theta^{(l)}}}\right)\\ &= \theta_1^{(l)}+\overline{\Delta\theta^{(l)}},\end{aligned} \tag{S10}$$

where in the second step we have defined the weighted average of the angular differences

$$\overline{\Delta\theta^{(l)}} = \frac{\sum_{i\in\mathcal{S}(\sigma)}\kappa_i^{\max(1,\beta)}\left(\theta_i^{(l)}-\theta_1^{(l)}\right)}{\sum_{i\in\mathcal{S}(\sigma)}\kappa_i^{\max(1,\beta)}}, \tag{S11}$$

which is assumed to be small. Eq. (S10) can be rewritten to obtain Eq. (S8). We generally choose Eq. (S8) as it respects the semi-group property explicitly, while Eq. (S9) only does so approximately in the case of small angular spread of the constituents as only then can one approximate

$$e^{\mathrm{i}\theta_\sigma^{(l+1)}} \approx \frac{\sum_{i\in S(\sigma)}(\kappa_i^{(l)})^{\max(1,\beta)}e^{\mathrm{i}\theta_i^{(l)}}}{\sum_{i\in S(\sigma)}(\kappa_i^{(l)})^{\max(1,\beta)}}, \tag{S12}$$

which is necessary for the semi-group property to hold.

The expected degree of a node with hidden degree $z=\kappa^{(l+1)}$ can be expressed as

$$\overline{k^{(l+1)}}(z) = \frac{N^{(l)}}{r}\int \mathrm{d}z'\int_0^\pi \mathrm{d}\theta\rho^{(l+1)}(z')\frac{1}{1+\frac{(R^{(l)}\theta)^\beta}{(\hat{\mu}^{(l)}zz')^{\max(1,\beta)}}} = \frac{N^{(l)}}{r}\int \mathrm{d}z'\rho^{(l+1)}(z')\,{}_2F_1\left[\begin{matrix}1,1/\beta\\1+1/\beta\end{matrix};-\frac{(\pi R^{(l)})^\beta}{(\hat{\mu}^{(l)}zz')^{\max(1,\beta)}}\right], \tag{S13}$$

where we know that for $x\to\infty$ one has ${}_2F_1(1,1/\beta,1+1/\beta,-x) = ((1-\beta)x)^{-1}+(\pi/\beta)\csc(\pi/\beta)x^{-1/\beta}+\mathcal{O}(x^{-2})$. Employing this approximation and using that $\langle\kappa^{(l+1)}\rangle = r^\xi\langle\kappa^{(l)}\rangle$, it can then be shown that

$$\overline{k^{(l+1)}}(\kappa^{(l+1)}) = r^{\xi-1}\frac{\langle k^{(l)}\rangle}{\langle\kappa^{(l)}\rangle}\kappa^{(l+1)}. \tag{S14}$$

We can then take the average over the hidden degree to get

$$\langle k^{(l+1)}\rangle = r^\nu\langle k^{(l)}\rangle, \tag{S15}$$

where we define $\nu = 2\xi-1$.

S2. SELF-SIMILARITY OF THE DEGREE DISTRIBUTION

The goal of this section is to find the degree distribution at the r'th level of renormalization. We start by studying the hidden degree distribution, assuming that in the original network the distribution is given by

$$\rho(\kappa) = \mathcal{N}\kappa^{-\gamma}, \qquad \kappa_0 \le \kappa \le \kappa_c, \tag{S16}$$

where $\mathcal{N}$ is the normalization constant. To obtain the distribution after renormalization we use Eq. (S6). Note that we change our method slightly from this point onward. Instead of looking at the l'th layer of the iterative normalization

procedure where each supernode is constructed with r nodes, we now study only a single normalization step. Note however that, due to the semi-group property, these two approaches are equivalent as l steps of size r can always be replaced by a single step of size r^l. We first find that the distribution $\tilde{\rho}(\tilde{\kappa})$, where $\tilde{\kappa} = \kappa^{\max(1,\beta)}$:

$$\tilde{\rho}(\tilde{\kappa}) = \tilde{\mathcal{N}}\tilde{\kappa}^{-\eta}, \qquad \tilde{\kappa}_0 \leq \tilde{\kappa} \leq \tilde{\kappa}_c, \tag{S17}$$

where we have defined $\tilde{\mathcal{N}} = \mathcal{N}/\max(1,\beta)$, $\tilde{\kappa}_0 = \kappa_0^{\max(1,\beta)}$, $\tilde{\kappa}_c = \kappa_c^{\max(1,\beta)}$ and $\eta = 1 + (\gamma-1)/\max(1,\beta)$. The next step is to find the distribution $\tilde{\rho}_r(\tilde{z})$ where $\tilde{z} = \sum_{i=1}^{r} \tilde{\kappa}_i$. We first state the result and follow with the proof:

$$\tilde{\rho}_r(\tilde{z}) = \sum_{n=1}^{r}\sum_{q=1}^{\infty} c_{n,q}\tilde{z}^{n(1-\eta)-q} 1_{[r\tilde{\kappa}_0, \tilde{\kappa}_c+(r-1)\tilde{\kappa}_0]}(\tilde{z}), \tag{S18}$$

where $c_{n,l}$ are constants. To obtain the distribution of the hidden degrees z in the renormalized layer, we use the fact that $z = \tilde{z}^{1/\max(1,\beta)}$, which leads to

$$\rho_r(z) = \max(1,\beta)\tilde{\rho}_r(z^{\max(1,\beta)})z^{\max(1,\beta)-1}. \tag{S19}$$

Note that for $\tilde{z} \gg 1$, the dominant scaling in Eq.(S18) is $\tilde{z}^{-\eta}$ ($n = 1, q = 1$). Plugging this into Eq.(S19) proves that the distribution $\rho_r(z)$ scales as $z^{-\gamma}$, which in turn demonstrates the self-similarity of the scaling behavior of the hidden degree distribution under renormalization. Note that the cut-off in the renormalized layer is given by $(\tilde{\kappa}_c + (r-1)\tilde{\kappa}_0)^{1/\max(1,\beta)}$, which is approximately κ_c if $\tilde{\kappa}_c \gg (r-1)\tilde{\kappa}_0$.

We now prove Eq. (S18) using induction. First, for $r = 2$, we know that the distribution $\tilde{\rho}_2(\tilde{z})$, where $\tilde{z} = \tilde{\kappa}_1 + \tilde{\kappa}_2$, is given by the convolution

$$\tilde{\rho}_2(\tilde{z}) = \int_{-\infty}^{\infty} \mathrm{d}\tilde{\kappa}\tilde{\rho}(\tilde{z}-\tilde{\kappa})\tilde{\rho}(\tilde{\kappa}). \tag{S20}$$

Taking into account the support of $\tilde{\rho}(\tilde{\kappa})$ we can conclude that $\tilde{\kappa}_0 \leq \tilde{z} - \tilde{\kappa} \leq \tilde{\kappa}_c$ and $\tilde{\kappa}_0 \leq \tilde{\kappa} \leq \tilde{\kappa}_c$. We then rewrite Eq. S20 as

$$\tilde{\rho}_2(\tilde{z}) = \frac{\tilde{\mathcal{N}}^2}{\tilde{z}^{2\gamma-1}}\left[\left(B_{1-\frac{\tilde{\kappa}_0}{\tilde{z}}}\begin{bmatrix}1-\eta\\1-\eta\end{bmatrix} - B_{\frac{\tilde{\kappa}_0}{\tilde{z}}}\begin{bmatrix}1-\eta\\1-\eta\end{bmatrix}\right)1_{[2\tilde{\kappa}_0, \tilde{\kappa}_c+\tilde{\kappa}_0]}(\tilde{z}) + \left(B_{\frac{\tilde{\kappa}_c}{\tilde{z}}}\begin{bmatrix}1-\eta\\1-\eta\end{bmatrix} - B_{1-\frac{\tilde{\kappa}_c}{\tilde{z}}}\begin{bmatrix}1-\eta\\1-\eta\end{bmatrix}\right)1_{[\tilde{\kappa}_0+\tilde{\kappa}_c, 2\tilde{\kappa}_c]}(\tilde{z})\right]. \tag{S21}$$

Here, $B_a\begin{bmatrix}b\\c\end{bmatrix}$ represents the incomplete beta function. We then note that this function can be expanded as

$$B_{1-x}\begin{bmatrix}a\\b\end{bmatrix} = \frac{\pi\csc(b\pi)}{a}\left(\sum_{n=0}^{\infty}\frac{a_{(n)}}{n!}(-x)^n\right) \times \left(\frac{\Gamma(1+a)}{\Gamma(a+b)}\sum_{q=0}^{\infty}\left[\frac{(b-1)_{(q)}(-a)_{(q)}}{q!\Gamma(1-b+q)}x^l\right]\right.$$

$$\left. - \frac{ax^b}{\Gamma(1-b)}\sum_{q=0}^{\infty}\left[\frac{(-a-b)_{(q)}}{q!\Gamma(1+b+q)}(-x)^q\right]\right) \tag{S22}$$

$$B_x\begin{bmatrix}a\\b\end{bmatrix} = x^a\sum_{n=0}^{\infty}\frac{(1-b)_{(n)}}{n!(a+n)}x^n \tag{S23}$$

when $x \to 0$, where the $y_{(n)}$ represent the falling factorials: $y_{(n)} = y(y-1)(y-2)...(y-n+1)$. In the case that $\tilde{z} \in [2\tilde{\kappa}_0, \tilde{\kappa}_c + \tilde{\kappa}_0]$, $\tilde{z}/\tilde{\kappa}_0 \ll 1$ in the tail of the distribution. Thus, we can apply the expansions given above and show that the dominant scaling in this regime is $\tilde{\rho}_2(\tilde{z}) \sim \tilde{z}^{-\eta}$ and that the full behavior is given by Eq. (S18). Crossing over to the regime $\tilde{z} \in [\tilde{\kappa}_0 + \tilde{\kappa}_c, 2\tilde{\kappa}_c]$, we get that $1 - \tilde{\kappa}_c/\tilde{z} \ll 1$, as least close to the transition. Using once again the series expansions of the beta functions we obtain that $\tilde{\rho}_2(z) \sim (1-\tilde{\kappa}_c/\tilde{z})^{1-\eta}$. This falls of hyperbolically and so we can take the probability density to be zero here. Therefore, we prove Eq. (S18) for $r = 2$.

Now, assuming that Eq. (S18) is true for some general r, let us investigate the case for $r+1$. In this case, we start with the convolution

$$\tilde{\rho}_{r+1}(\tilde{z}) = \int_{r\tilde{\kappa}_0}^{\tilde{z}-\tilde{\kappa}_0}\mathrm{d}\tilde{\kappa}\rho_1(\tilde{z}-\tilde{\kappa})\rho_r(\tilde{\kappa})1_{[(r+1)\tilde{\kappa}_0, \tilde{\kappa}_c+r\tilde{\kappa}_0]}(\tilde{z})$$

$$+ \int_{\tilde{z}-\tilde{\kappa}_c}^{\tilde{\kappa}_c+(r-1)\tilde{\kappa}_0}\mathrm{d}\tilde{\kappa}\tilde{\rho}_1(\tilde{z}-\tilde{\kappa})\tilde{\rho}_r(\tilde{\kappa})1_{[\tilde{\kappa}_c+r\tilde{\kappa}_0, 2\tilde{\kappa}_c+(r-1)\tilde{\kappa}_0]}(\tilde{z}), \tag{S24}$$

where have taken into account the respective domains of the two functions $\tilde{\rho}_1$ and $\tilde{\rho}_r$. The fact that $\tilde{\rho}_r(\tilde{z})$ can be expanded into a sum of terms $\tilde{g}_r(\tilde{z};\alpha) \sim \tilde{z}^{-\alpha}$, where $\alpha \geq \eta$, implies that $\tilde{\rho}_{r+1}(\tilde{z})$ can be expanded into a sum of integrals $\tilde{I}(\tilde{z};\alpha)$ evaluating to

$$\begin{aligned}\tilde{I}(\tilde{z};\alpha) = \tilde{\mathcal{N}}^r\, \tilde{z}^{1-\eta-\alpha} \Bigg[\left(B_{1-\frac{\tilde{\kappa}_0}{\tilde{z}}} \begin{bmatrix} 1-\alpha \\ 1-\eta \end{bmatrix} - \; B_{\frac{r\tilde{\kappa}_0}{\tilde{z}}} \begin{bmatrix} 1-\alpha \\ 1-\eta \end{bmatrix} \right) 1_{[(r+1)\tilde{\kappa}_0, \tilde{\kappa}_c + r\tilde{\kappa}_0]} \\ + \left(B_{\frac{\tilde{\kappa}_c + (r-1)\tilde{\kappa}_0}{\tilde{z}}} \begin{bmatrix} 1-\alpha \\ 1-\eta \end{bmatrix} - B_{1-\frac{\tilde{\kappa}_c}{\tilde{z}}} \begin{bmatrix} 1-\alpha \\ 1-\eta \end{bmatrix} \right) 1_{[\tilde{\kappa}_c + r\tilde{\kappa}_0, 2\tilde{\kappa}_c + (r-1)\tilde{\kappa}_0]} \Bigg]. \end{aligned} \tag{S25}$$

Using the same arguments as before, we can show that $\forall \alpha$ the integral falls off hyperbolically in the second region. When $\tilde{z} \in [(r+1)\tilde{\kappa}_0, \tilde{\kappa}_c + r\tilde{\kappa}_0]$, it can be shown that the expression can be rewritten in the form of Eq. (S18), where the dominant scaling for large $\tilde{z}$ is once again $\sim \tilde{z}^{-\eta}$. With this we conclude the proof.

Note that this proof is contingent on some assumptions, most notably that $r\tilde{\kappa}_0 \ll \tilde{\kappa}_c$. Of course, for finite $\tilde{\kappa}_c$, there is always an r for which this assumption breaks down. This has to do with the central limit theorem: For a finite cut-off $\tilde{\kappa}_c$, the variance of the distribution $\tilde{\rho}(\tilde{\kappa})$ is also finite, and thus the distribution $\tilde{\rho}_r(\tilde{z})$ necessarily approaches a Gaussian as $r \to \infty$. In the case of the model we in general assume that $\tilde{\kappa}_c = \tilde{\kappa}_0 N^{\max(1,\beta)/(\gamma-1)}$, which is very large for the network sizes we typically work with, and so one can perform several renormalization steps before one 'feels' the effect of the cut-off.

It is known that the degree distribution is related to the distribution of hidden degrees by

$$P_r(k) = \frac{1}{k!} \int \mathrm{d}z \rho(z) \overline{k}(z)^k e^{-\overline{k}(z)}, \tag{S26}$$

where $\overline{k}(\kappa)$ is the expected degree of a node with hidden degree κ. In the unrenormalized layer one can show that $\overline{k}(\kappa) = \kappa$ when $\hat{\mu}$ is chosen correctly. For this to be true for in the renormalized layer, however, one would need that $\langle \kappa_r \rangle = \langle k_r \rangle$, which is not generally the case as the scaling exponents determining the flow of these two quantities, ξ and ν, are not always equal. Using Eq. (S14) and $\xi = (\nu+1)/2$, one obtains that

$$\overline{k_r}(\kappa_r) = r^{(\nu-1)/2} \kappa_r \tag{S27}$$

We now note that we do not know the exact functional form of $\rho_r(\kappa)$, at least not for $\beta > 1$. To be able to plug in Eq. (S18), we first need to transform (S26). It can be shown that this integral is equivalent to

$$P_r(k) = \frac{1}{k!} \int_{r\tilde{\kappa}_0}^{\tilde{\kappa}_c + (r-1)\tilde{\kappa}_0} \mathrm{d}\tilde{z} \frac{r^{k(\nu-1)/2} \tilde{\rho}_r(\tilde{z}) \tilde{z}^{\frac{k}{\max(1,\beta)}}}{\exp\left(r^{(\nu-1)/2} \tilde{z}^{\frac{1}{\max(1,\beta)}} \right)}. \tag{S28}$$

Then, combining the previous result with Eq. (S18) and Eq. (S26) one obtains

$$\begin{aligned} P_r(k) &= \sum_{n=1}^{r} \sum_{q=1}^{\infty} \frac{c_{n,q} r^{k\frac{\nu-1}{2}}}{k!} \int_{r\tilde{\kappa}_0}^{\tilde{\kappa}_c + (r-1)\tilde{\kappa}_0} \mathrm{d}\tilde{z} \frac{\tilde{z}^{n(1-\eta)-q+k/\max(1,\beta)}}{\exp\left(r^{\frac{\nu-1}{2}} \tilde{z}^{1/\max(1,\beta)} \right)} \\ &= \sum_{n=1}^{r} \sum_{q=1}^{\infty} \frac{c_{n,l} \max(1,\beta) r^{\frac{\nu-1}{2}(\max(1,\beta)(1-q)+n(1-\gamma))}}{k!} \Bigg[\Gamma\left(\max(1,\beta)(1-q) + n(1-\gamma) + k, r^{\frac{\nu-1}{2}+1/\max(1,\beta)} \kappa_0 \right) \\ &\quad + \Gamma\left(\max(1,\beta)(1-q) + n(1-\gamma) + k, r^{\frac{\nu-1}{2}} \left(\tilde{\kappa}_c + (r-1)\tilde{\kappa}_0 \right)^{1/\max(1,\beta)} \right) \Bigg]. \end{aligned} \tag{S29}$$

When $k \gg \left(\tilde{\kappa}_c + (r-1)\tilde{\kappa}_0 \right)^{1/\max(1,\beta)}$, the two gamma functions cancel, meaning that the probability density vanishes. When $r^{1/\max(1,\beta)} \kappa_0 \ll k \leq \left(\tilde{\kappa}_c + (r-1)\tilde{\kappa}_0 \right)^{1/\max(1,\beta)}$, the first term scales as $k^{-\gamma}$, whereas the second term falls off exponentially. This implies that the scaling behavior of the tail of the distribution is preserved under renormalization. Note that once again for large κ_c the cut-off does not evolve under renormalization.

S3. REAL NETWORKS

In this section we show the results of the RG procedure applied to a set of Real Networks living in the weakly geometric region $\beta < 1$. We present here short descriptions of these networks as given in Ref. [2]. The properties of these networks are shown in Tab. S1.

- **Foodweb–Eocene** [3]: A reconstructed food web of an ecosystem from the early Eocene (48 million years ago). Nodes represent taxa and edges represent consumer-resource relations. The original network was directed.
- **WordAdjacency–English** [4]: A network of word adjacency in English texts. Nodes represent words and two words are connected if one directly follows the other in texts. The original network was directed.
- **WordAdjacency–Japanese** [4]: A network of word adjacency in Japanese texts. Nodes represent words and two words are connected if one directly follows the other in texts. The original network was directed.
- **MB–R.norvegicus** [5]: A metabolic network of the rat (Ratus norvegicus), extracted from the Kyoto Encyclopedia of Genes and Genomes (KEGG). Nodes represent substances involved in enzymatic reactions and edges represent reactant-product pairs.
- **WikiTalk–Catalan** [6]: A network where nodes represents Wikipedia editors for a certain language (in this case Catalan), and where user i and j are connected if i leaves a message on the talk page of j. The original network was directed.
- **GI–S.cerevisiae** [7]: A network based on the Molecular Interaction Search Tool (MIST) for baker's yeast (Saccharomyces cerevisiae). Here node represent genes and the edges indicate that the effects of mutations in one gene can be modified by mutations of another gene.
- **GMP–C.elegans** [8]: A multiplex network representing different types of genetic interactions for the nematode worm Caenorhabditis elegans. The layers represent physical, association, co-localization, direct, suppressive and additive interactions. In this paper we create a monolayer network by treating the different interaction types equally and removing repeated links. The original network was directed.
- **Gnutella** [9]: A snapshot of the Gnutella peer-to-peer file sharing network on August 4th 2002. Nodes are hosts and edges are connections between them. The original network was directed.
- **PPI–S.cerevisiae** [7]: A network based on the Molecular Interaction Search Tool (MIST) for baker's yeast (Saccharomyces cerevisiae). Here node represent genes and the edges indicate that there are physical interactions between their associated proteins.
- **PPI–D.melanogaster** [7]: A network based on the Molecular Interaction Search Tool (MIST) for the fruit fly (Drosophila melanogaster). Here node represent genes and the edges indicate that there are physical interactions between their associated proteins.
- **Transport–London** [10]: An multiplex network of the public transportation system in London. Nodes are London train stations and the links can represent either the underground, overground and DLR connections. There connections are treated equally as to create a mono-layer network.
- **GMP–S.cerevisiae** [8]: A multiplex network representing different types of genetic interactions for baker's yeast (Saccharomyces cerevisiae). The layers represent physical, association, co-localization, direct, suppressive and additive interactions. In this paper we create a monolayer network by treating the different interaction types equally and removing repeated links. The original network was directed.
- **Internet-PoP** [11]: The Kentucky Datalink network, an internet graph at the Point of Presence (PoP) level. Nodes are physical network interface points and links physical connections between them.
- **PPI–H.sapiens** [7]: A network based on the Molecular Interaction Search Tool (MIST) for humans (Homo sapiens). Here node represent genes and the edges indicate that there are physical interactions between their associated proteins.
- **WikiVote** [12]: The network represents the voting process used to select Wikipedia administrators, which are contributors with access to additional technical features. Nodes represents Wikipedia users and an edge is created if user i votes on the selections of user j. The original network was directed.
- **MathOverflow** [13]: An interaction network of users (nodes) on the online Q&A site MathOverflow. An edge from node i to node j indicates that i responded to an answer by j. The original network was directed.

TABLE S1. Network properties of several real weakly geometric networks shown. The following abbreviations are used: (MB) Metabolic, (GI) Genetic Interactions, (GMP) Genetic Multiplex, (PPI) Protein Protein Interactions, (PoP) Point of Presence.

Network	**Area**	N	$\langle k \rangle$	$k_{\max}$	$\bar{c}$	β
Foodweb–Eocene	Ecological	700	18.3	192	0.10	$\beta \approx 0$
WordAdjacency–English	Language	7377	12.0	2568	0.47	$\beta \approx 0$
WordAdjacency–Japanese	Language	2698	5.9	725	0.30	$\beta \approx 0$
MB–R.norvegicus	Cell	1590	5.9	498	0.19	$\beta \approx 0$
WikiTalk–Catalan	Social	79209	4.6	53234	0.83	$\beta \approx 0$
GI–S.cerevisiae	Cell	5933	149	2244	0.17	0.63
GMP–C.elegans	Cell	3692	4.1	526	0.11	0.69
Gnutella	Technological	10876	7.4	103	0.01	0.73
PPI–S.cerevisiae	Cell	7271	45.0	3613	0.37	0.75
PPI–D.melanogaster	Cell	11319	23.7	889	0.10	0.84
Transport–London	Transportation	369	2.3	7	0.03	0.86
GMP–S.cerevisiae	Cell	6567	68.1	3254	0.22	0.88
Internet-PoP	Technological	754	2.4	7	0.03	0.90
PPI–H.sapiens	Cell	27578	37.9	2883	0.15	0.91
WikiVote	Social	7066	28.5	1065	0.21	0.91
MathOverflow	Social	13599	10.5	949	0.32	0.99

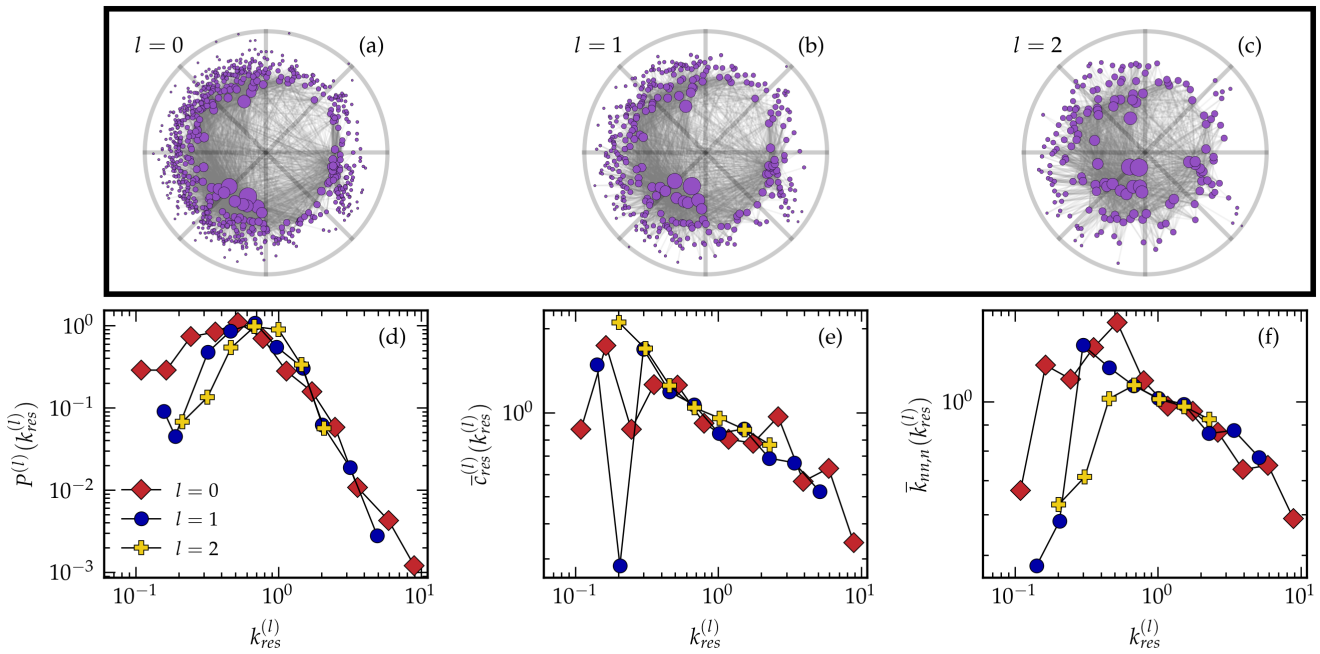

FIG. S1. Summary of the results of GR for the Foodweb-Eocene network. **(a-c)** Representation of the embedding for layers $l = 1, 2$ and 3 in the hyperbolic plane. The top 50% most geometric edges are shown. The topological properties are also given: **(d)** the degree distribution, where $k_{res}^{(l)} = k^{(l)}/\langle k^{(l)} \rangle$, **(e)** the rescaled average local clustering coefficient per degree class, where $\bar{c}_{res}^{(l)}(k^{(l)}) = \bar{c}^{(l)}(k^{(l)})/\bar{c}^{(l)}$ and finally **(f)** the degree-degree correlations per degree class. In all cases we log-bin the degrees.

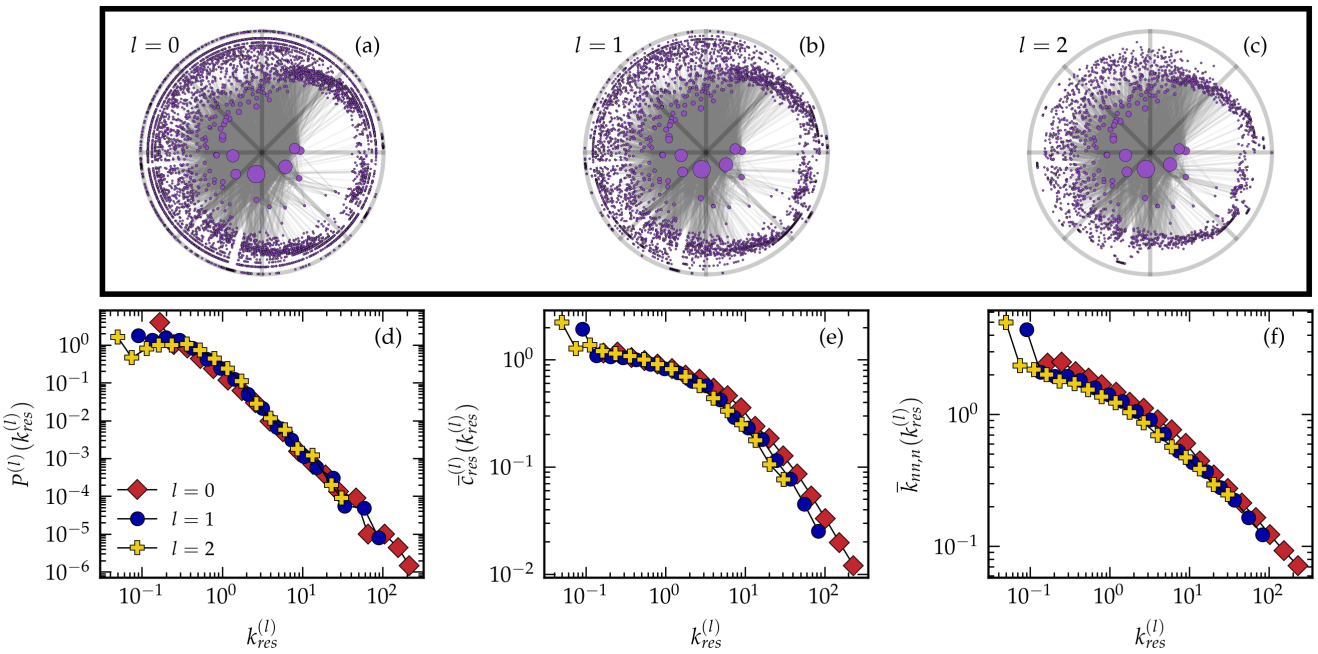

FIG. S2. Summary of the results of GR for the WordAdjacency-English network. **(a-c)** Representation of the embedding for layers $l = 1, 2$ and 3 in the hyperbolic plane. The top 10% most geometric edges are shown. The topological properties are also given: **(d)** the degree distribution, where $k^{(l)}_{res} = k^{(l)}/\langle k^{(l)}\rangle$, **(e)** the rescaled average local clustering coefficient per degree class, where $\bar{c}^{(l)}_{res}(k^{(l)}) = \bar{c}^{(l)}(k^{(l)})/\bar{c}^{(l)}$ and finally **(f)** the degree-degree correlations per degree class. In all cases we log-bin the degrees.

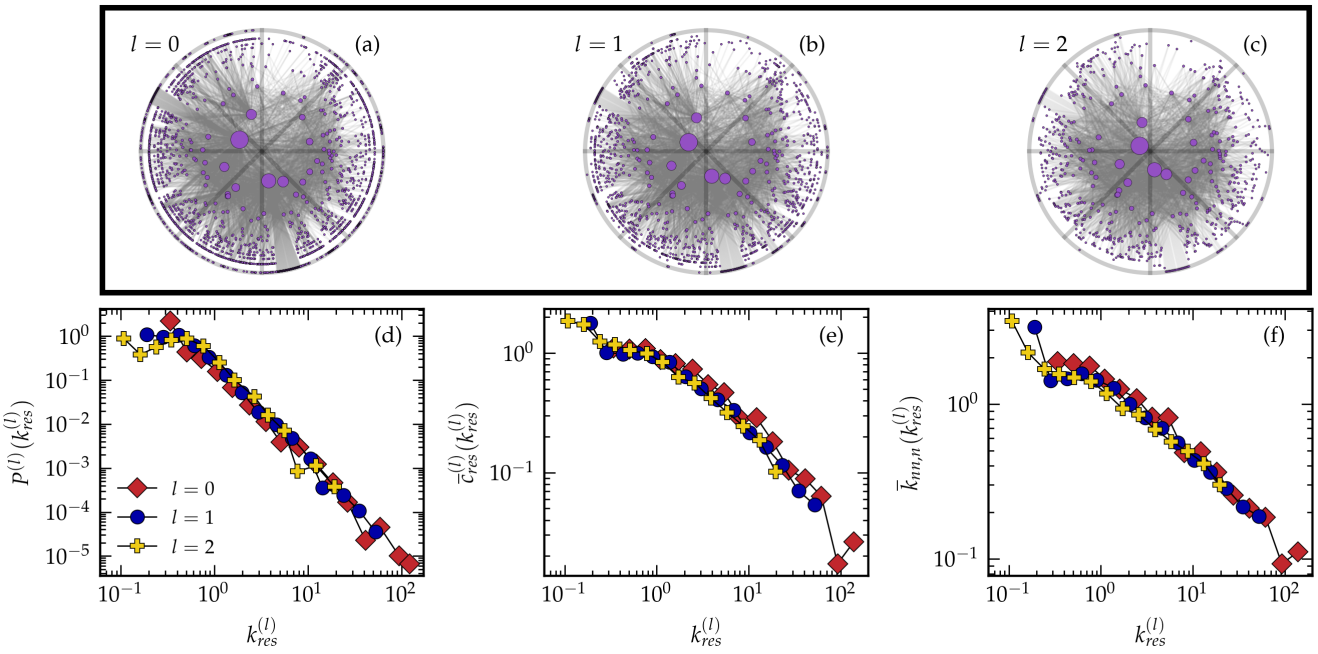

FIG. S3. Summary of the results of GR for the WordAdjacency–Japanese network. **(a-c)** Representation of the embedding for layers $l = 1, 2$ and 3 in the hyperbolic plane. The top 50% most geometric edges are shown. The topological properties are also given: **(d)** the degree distribution, where $k^{(l)}_{res} = k^{(l)}/\langle k^{(l)}\rangle$, **(e)** the rescaled average local clustering coefficient per degree class, where $\bar{c}^{(l)}_{res}(k^{(l)}) = \bar{c}^{(l)}(k^{(l)})/\bar{c}^{(l)}$ and finally **(f)** the degree-degree correlations per degree class. In all cases we log-bin the degrees.

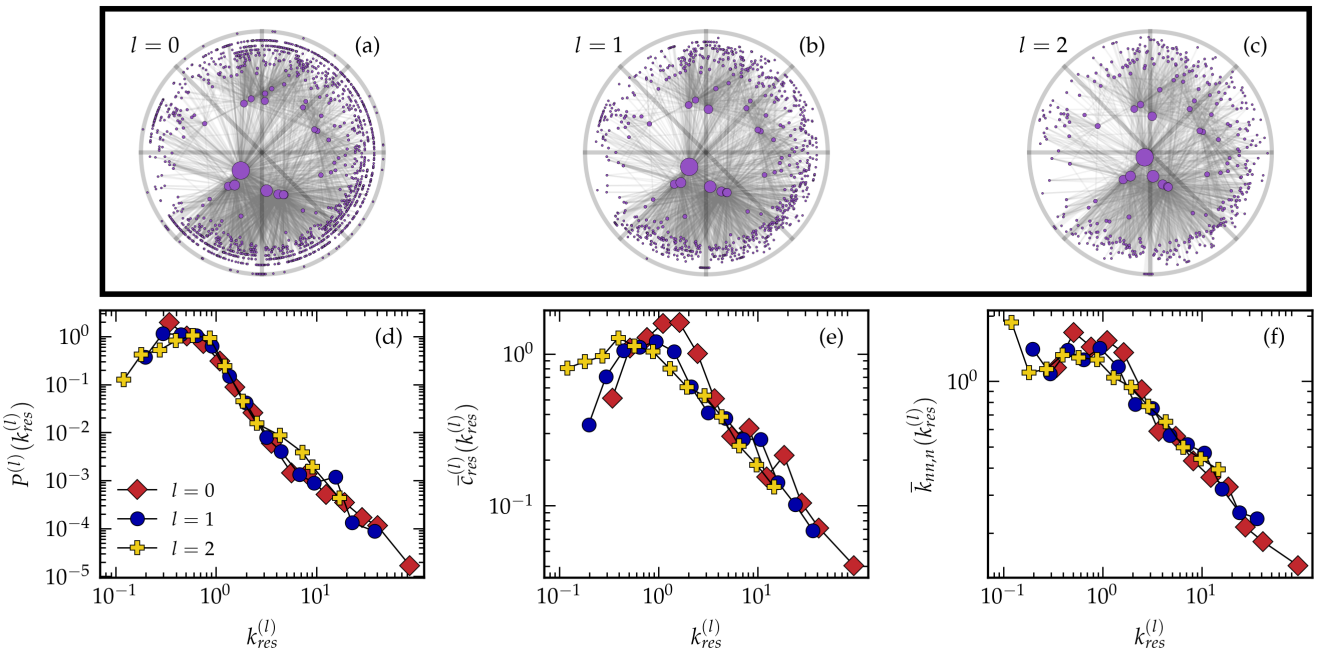

FIG. S4. Summary of the results of GR for the MB–R.norvegicus network. **(a-c)** Representation of the embedding for layers $l = 1, 2$ and 3 in the hyperbolic plane. The top 50% most geometric edges are shown. The topological properties are also given: **(d)** the degree distribution, where $k^{(l)}_{res} = k^{(l)}/\langle k^{(l)} \rangle$, **(e)** the rescaled average local clustering coefficient per degree class, where $\bar{c}^{(l)}_{res}(k^{(l)}) = \bar{c}^{(l)}(k^{(l)})/\bar{c}^{(l)}$ and finally **(f)** the degree-degree correlations per degree class. In all cases we log-bin the degrees.

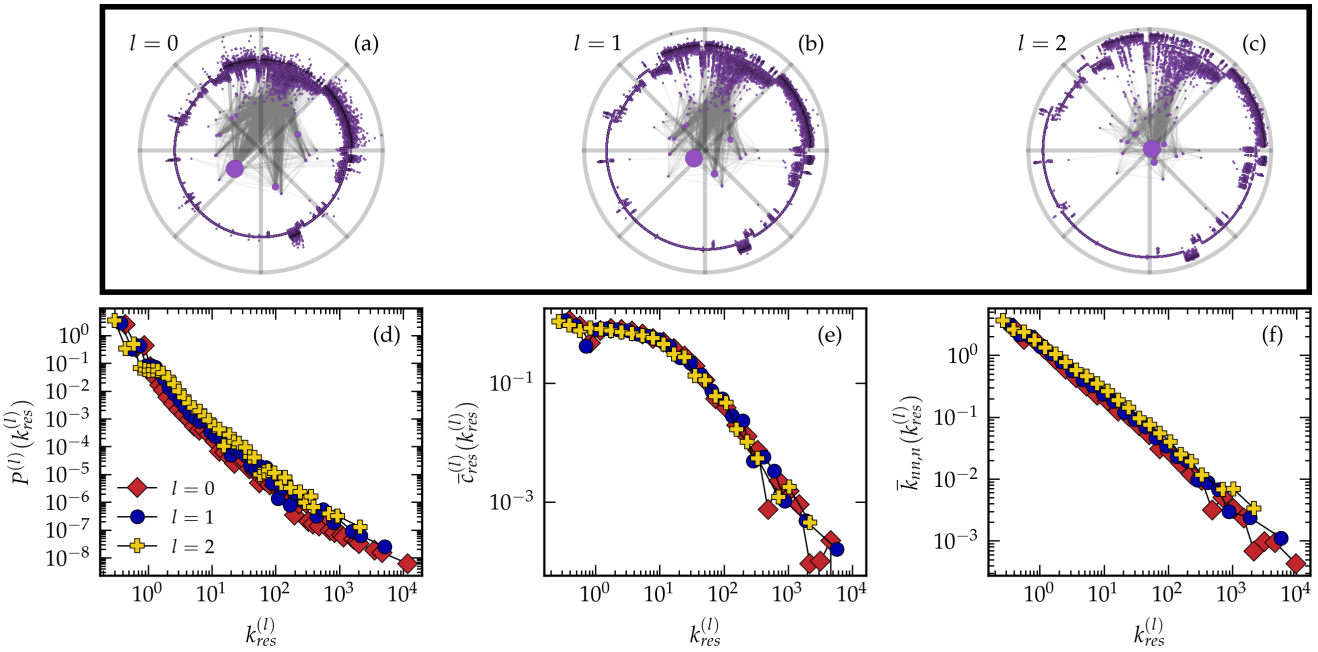

FIG. S5. Summary of the results of GR for the WikiTalk–Catalan network. **(a-c)** Representation of the embedding for layers $l = 1, 2$ and 3 in the hyperbolic plane. The top 1% most geometric edges are shown. The topological properties are also given: **(d)** the degree distribution, where $k^{(l)}_{res} = k^{(l)}/\langle k^{(l)} \rangle$, **(e)** the rescaled average local clustering coefficient per degree class, where $\bar{c}^{(l)}_{res}(k^{(l)}) = \bar{c}^{(l)}(k^{(l)})/\bar{c}^{(l)}$ and finally **(f)** the degree-degree correlations per degree class. In all cases we log-bin the degrees.

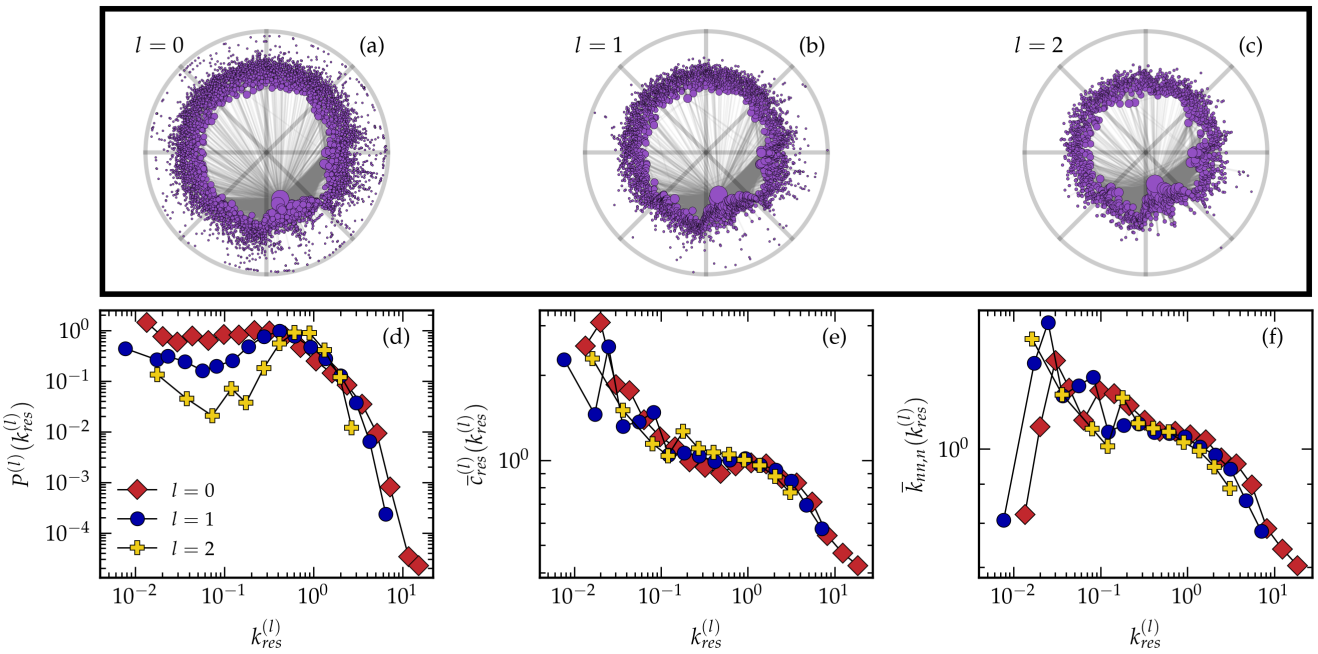

FIG. S6. Summary of the results of GR for the GI–S.cerevisiae network. **(a-c)** Representation of the embedding for layers $l = 1, 2$ and 3 in the hyperbolic plane. The top 5% most geometric edges are shown. The topological properties are also given: **(d)** the degree distribution, where $k^{(l)}_{res} = k^{(l)}/\langle k^{(l)}\rangle$, **(e)** the rescaled average local clustering coefficient per degree class, where $\overline{c}^{(l)}_{res}(k^{(l)}) = \overline{c}^{(l)}(k^{(l)})/\overline{c}^{(l)}$ and finally **(f)** the degree-degree correlations per degree class. In all cases we log-bin the degrees.

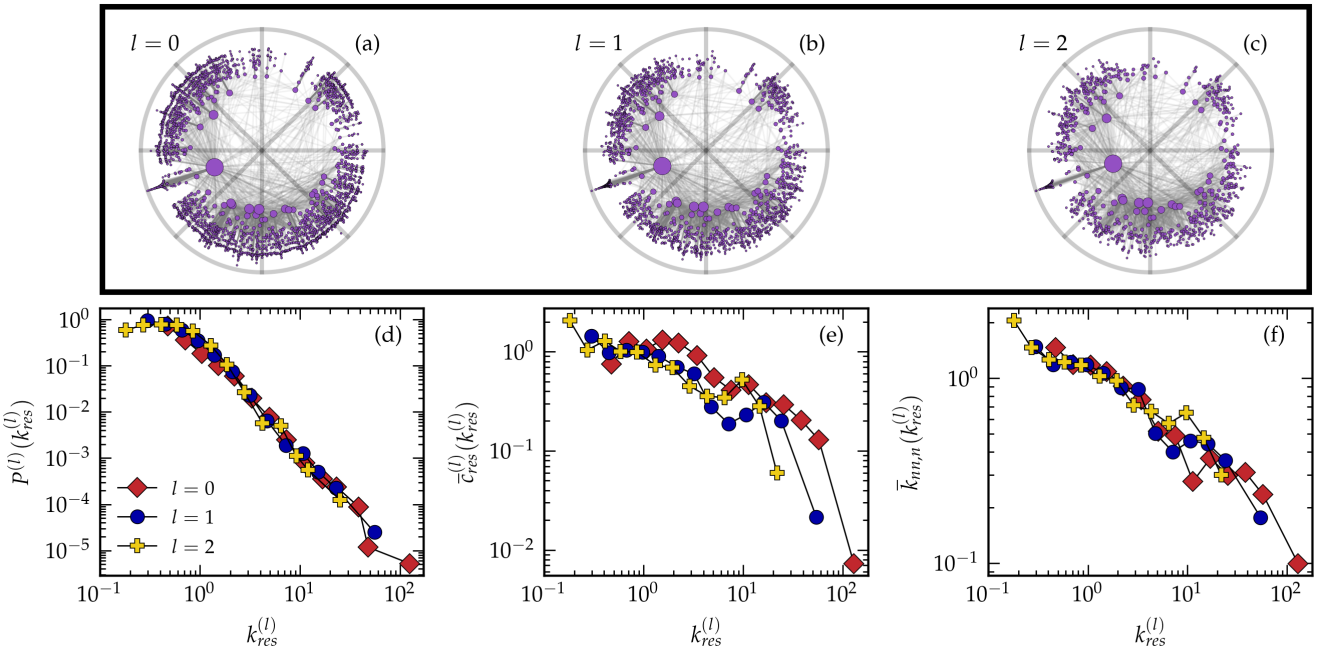

FIG. S7. Summary of the results of GR for the GMP–C.elegans network. **(a-c)** Representation of the embedding for layers $l = 1, 2$ and 3 in the hyperbolic plane. The top 50% most geometric edges are shown. The topological properties are also given: **(d)** the degree distribution, where $k^{(l)}_{res} = k^{(l)}/\langle k^{(l)}\rangle$, **(e)** the rescaled average local clustering coefficient per degree class, where $\overline{c}^{(l)}_{res}(k^{(l)}) = \overline{c}^{(l)}(k^{(l)})/\overline{c}^{(l)}$ and finally **(f)** the degree-degree correlations per degree class. In all cases we log-bin the degrees.

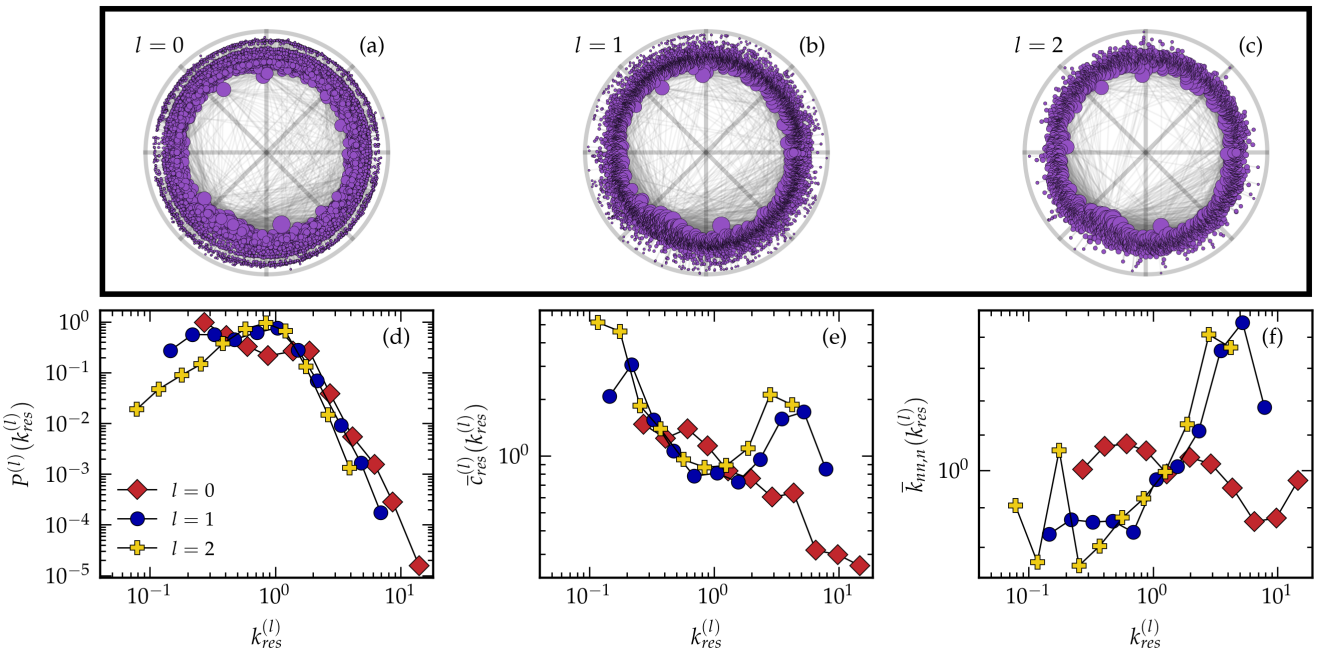

FIG. S8. Summary of the results of GR for the Gnutella network. **(a-c)** Representation of the embedding for layers $l = 1, 2$ and 3 in the hyperbolic plane. The top 40% most geometric edges are shown. The topological properties are also given: **(d)** the degree distribution, where $k^{(l)}_{res} = k^{(l)}/\langle k^{(l)}\rangle$, **(e)** the rescaled average local clustering coefficient per degree class, where $\bar{c}^{(l)}_{res}(k^{(l)}) = \bar{c}^{(l)}(k^{(l)})/\bar{c}^{(l)}$ and finally **(f)** the degree-degree correlations per degree class. In all cases we log-bin the degrees.

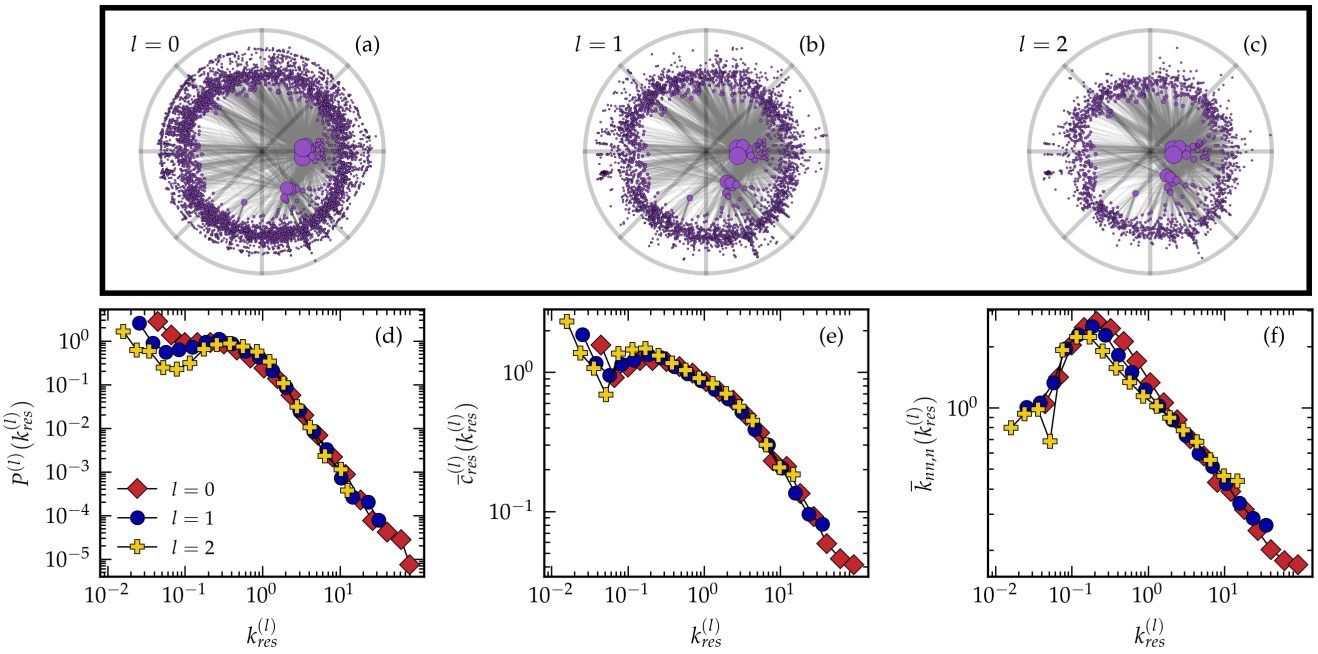

FIG. S9. Summary of the results of GR for the PPI–S.cerevisiae network. **(a-c)** Representation of the embedding for layers $l = 1, 2$ and 3 in the hyperbolic plane. The top 3% most geometric edges are shown. The topological properties are also given: **(d)** the degree distribution, where $k^{(l)}_{res} = k^{(l)}/\langle k^{(l)}\rangle$, **(e)** the rescaled average local clustering coefficient per degree class, where $\bar{c}^{(l)}_{res}(k^{(l)}) = \bar{c}^{(l)}(k^{(l)})/\bar{c}^{(l)}$ and finally **(f)** the degree-degree correlations per degree class. In all cases we log-bin the degrees.

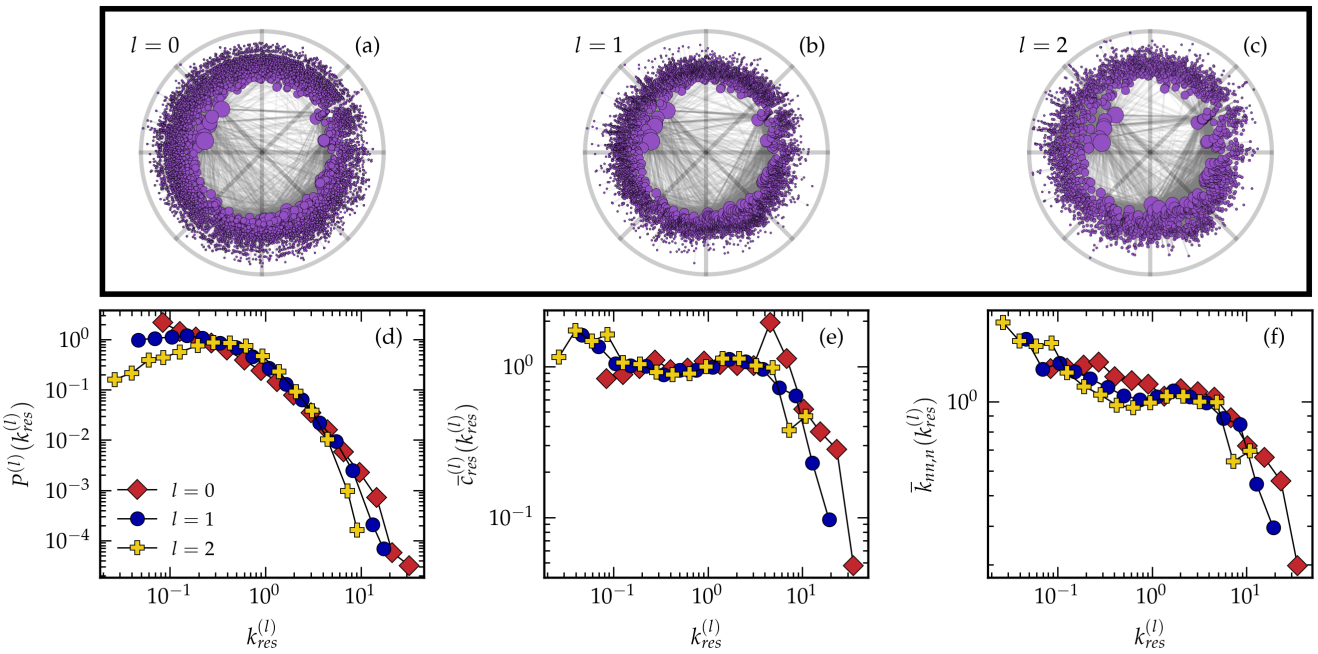

FIG. S10. Summary of the results of GR for the PPI–D.melanogaster network. **(a-c)** Representation of the embedding for layers $l = 1, 2$ and 3 in the hyperbolic plane. The top 20% most geometric edges are shown. The topological properties are also given: **(d)** the degree distribution, where $k^{(l)}_{res} = k^{(l)}/\langle k^{(l)}\rangle$, **(e)** the rescaled average local clustering coefficient per degree class, where $\bar{c}^{(l)}_{res}(k^{(l)}) = \bar{c}^{(l)}(k^{(l)})/\bar{c}^{(l)}$ and finally **(f)** the degree-degree correlations per degree class. In all cases we log-bin the degrees.

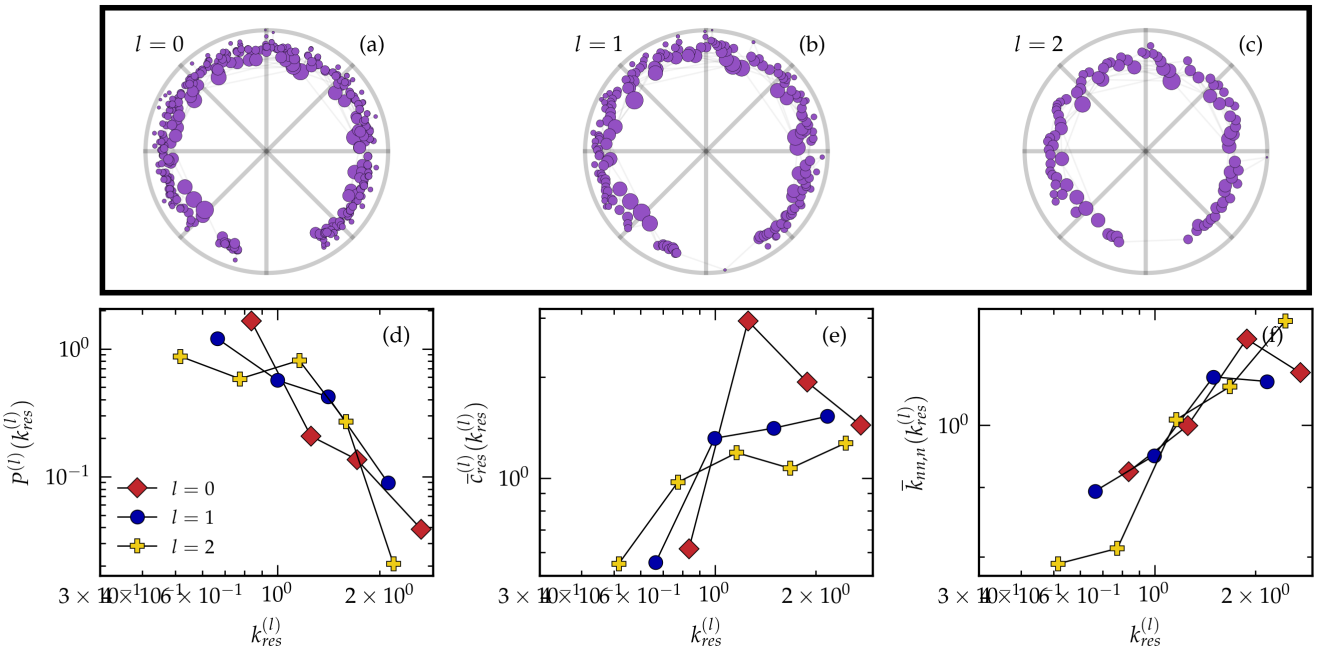

FIG. S11. Summary of the results of GR for the Transport–London network. **(a-c)** Representation of the embedding for layers $l = 1, 2$ and 3 in the hyperbolic plane. The top 100% most geometric edges are shown. The topological properties are also given: **(d)** the degree distribution, where $k^{(l)}_{res} = k^{(l)}/\langle k^{(l)}\rangle$, **(e)** the rescaled average local clustering coefficient per degree class, where $\bar{c}^{(l)}_{res}(k^{(l)}) = \bar{c}^{(l)}(k^{(l)})/\bar{c}^{(l)}$ and finally **(f)** the degree-degree correlations per degree class. In all cases we log-bin the degrees.

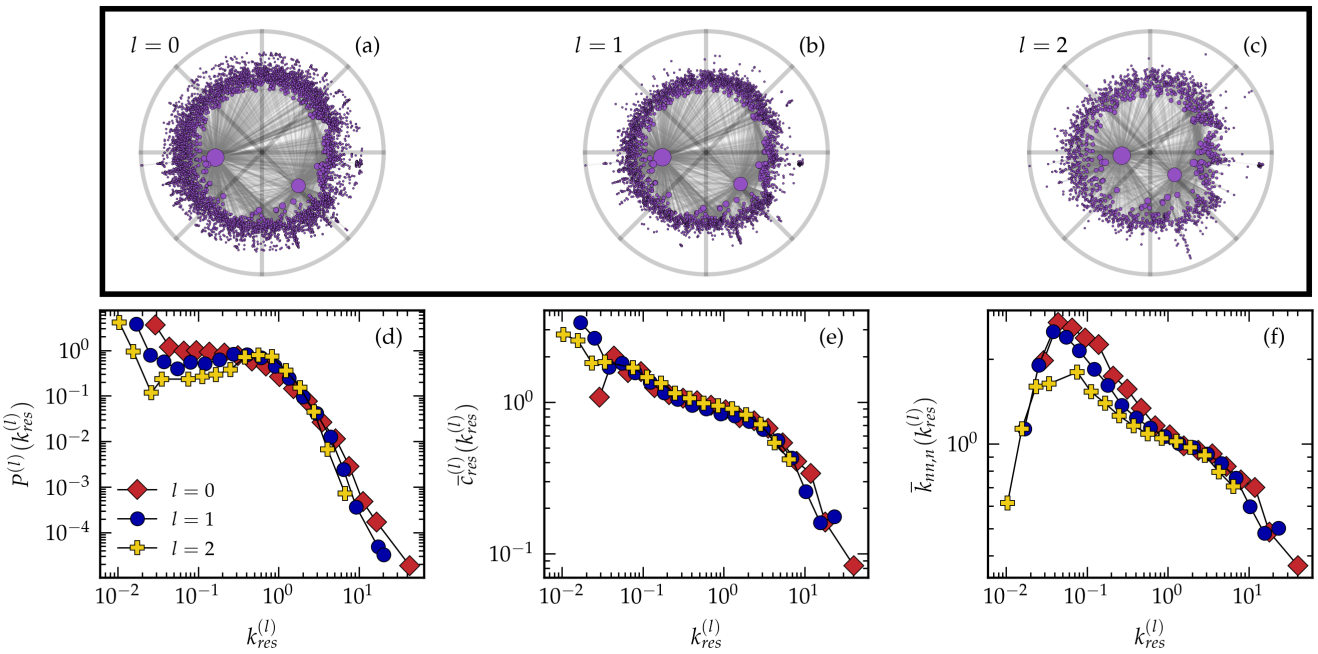

FIG. S12. Summary of the results of GR for the GMP–S.cerevisiae network. **(a-c)** Representation of the embedding for layers $l = 1, 2$ and 3 in the hyperbolic plane. The top 5% most geometric edges are shown. The topological properties are also given: **(d)** the degree distribution, where $k^{(l)}_{res} = k^{(l)}/\langle k^{(l)}\rangle$, **(e)** the rescaled average local clustering coefficient per degree class, where $\bar{c}^{(l)}_{res}(k^{(l)}) = \bar{c}^{(l)}(k^{(l)})/\bar{c}^{(l)}$ and finally **(f)** the degree-degree correlations per degree class. In all cases we log-bin the degrees.

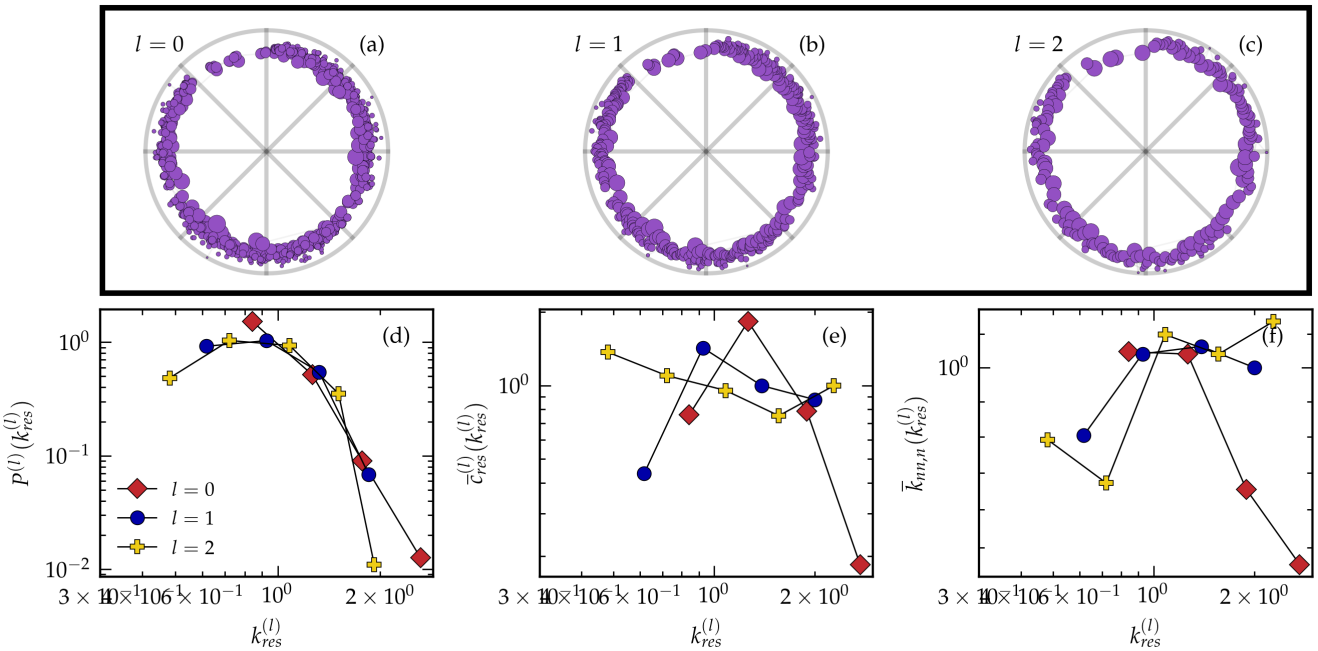

FIG. S13. Summary of the results of GR for the Internet-PoP network. **(a-c)** Representation of the embedding for layers $l = 1, 2$ and 3 in the hyperbolic plane. The top 100% most geometric edges are shown. The topological properties are also given: **(d)** the degree distribution, where $k^{(l)}_{res} = k^{(l)}/\langle k^{(l)}\rangle$, **(e)** the rescaled average local clustering coefficient per degree class, where $\bar{c}^{(l)}_{res}(k^{(l)}) = \bar{c}^{(l)}(k^{(l)})/\bar{c}^{(l)}$ and finally **(f)** the degree-degree correlations per degree class. In all cases we log-bin the degrees.

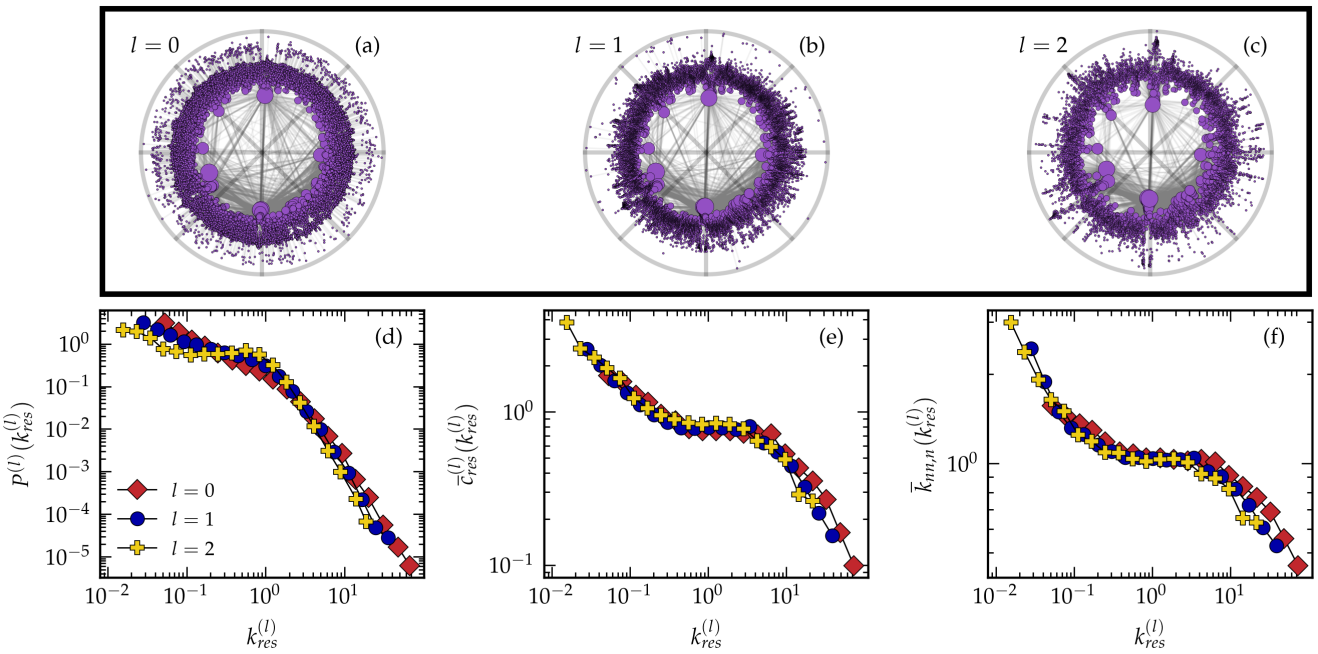

FIG. S14. Summary of the results of GR for the PPI–H.sapiens network. **(a-c)** Representation of the embedding for layers $l = 1, 2$ and 3 in the hyperbolic plane. The top 5% most geometric edges are shown. The topological properties are also given: **(d)** the degree distribution, where $k^{(l)}_{res} = k^{(l)}/\langle k^{(l)}\rangle$, **(e)** the rescaled average local clustering coefficient per degree class, where $\overline{c}^{(l)}_{res}(k^{(l)}) = \overline{c}^{(l)}(k^{(l)})/\overline{c}^{(l)}$ and finally **(f)** the degree-degree correlations per degree class. In all cases we log-bin the degrees.

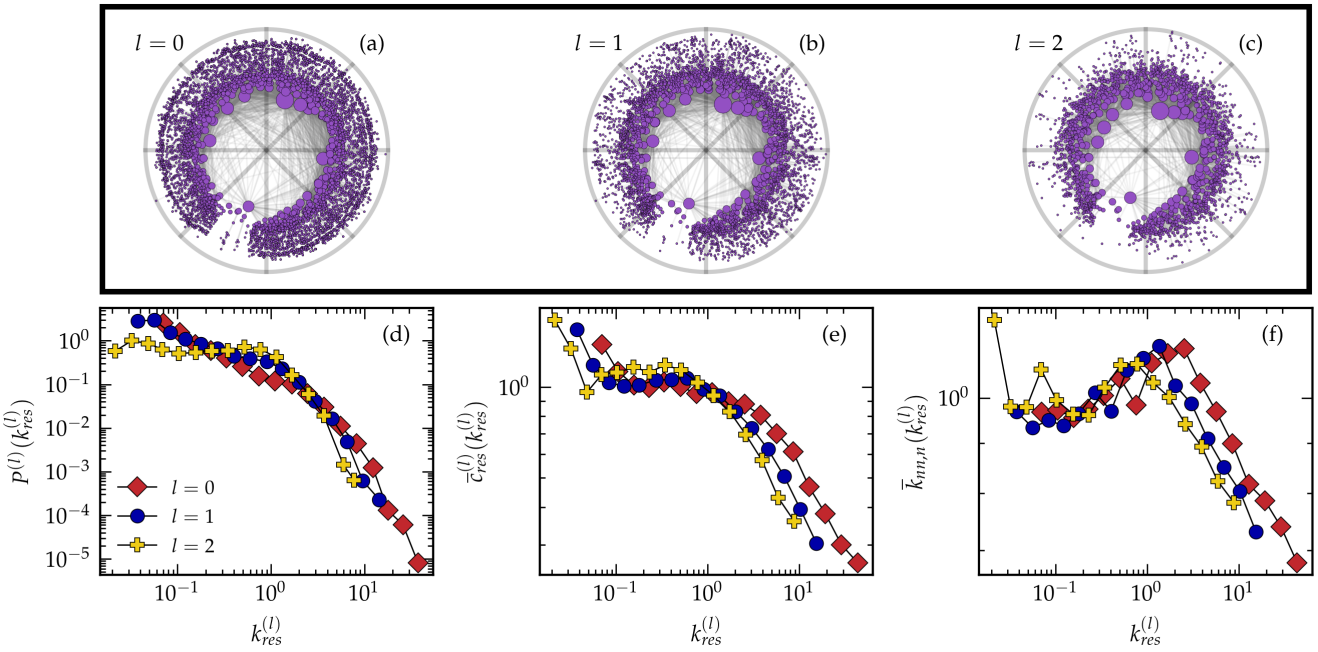

FIG. S15. Summary of the results of GR for the WikiVote network. **(a-c)** Representation of the embedding for layers $l = 1, 2$ and 3 in the hyperbolic plane. The top 10% most geometric edges are shown. The topological properties are also given: **(d)** the degree distribution, where $k^{(l)}_{res} = k^{(l)}/\langle k^{(l)}\rangle$, **(e)** the rescaled average local clustering coefficient per degree class, where $\overline{c}^{(l)}_{res}(k^{(l)}) = \overline{c}^{(l)}(k^{(l)})/\overline{c}^{(l)}$ and finally **(f)** the degree-degree correlations per degree class. In all cases we log-bin the degrees.

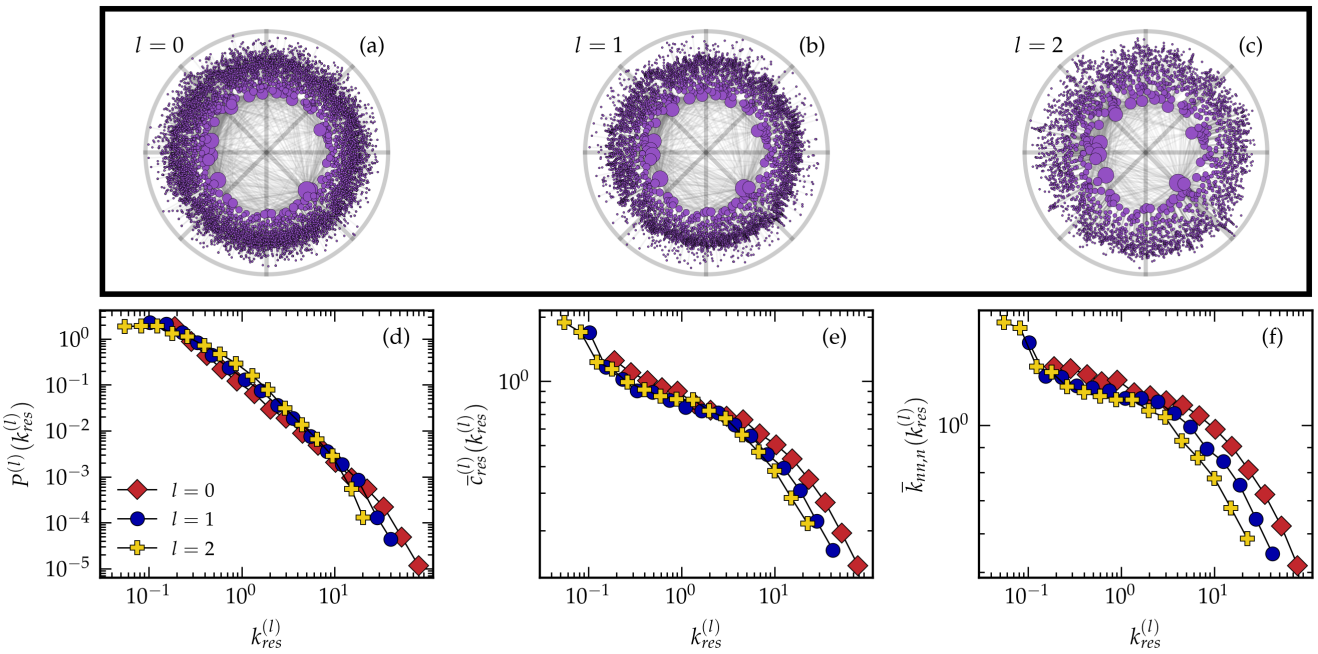

FIG. S16. Summary of the results of GR for the MathOverflow network. **(a-c)** Representation of the embedding for layers $l = 1, 2$ and 3 in the hyperbolic plane. The top 5% most geometric edges are shown. The topological properties are also given: **(d)** the degree distribution, where $k^{(l)}_{res} = k^{(l)}/\langle k^{(l)} \rangle$, **(e)** the rescaled average local clustering coefficient per degree class, where $\bar{c}^{(l)}_{res}(k^{(l)}) = \bar{c}^{(l)}(k^{(l)})/\bar{c}^{(l)}$ and finally **(f)** the degree-degree correlations per degree class. In all cases we log-bin the degrees.

[1] G. García-Pérez, M. Boguñá, and M. Á. Serrano, Multiscale unfolding of real networks by geometric renormalization, Nature Physics **14**, 583 (2018).

[2] J. van der Kolk, M. Á. Serrano, and M. Boguñá, Random graphs and real networks with weak geometric coupling (2023), arXiv:2312.07416 [physics.soc-ph].

[3] J. A. Dunne, C. C. Labandeira, and R. J. Williams, Highly resolved early eocene food webs show development of modern trophic structure after the end-cretaceous extinction, Proceedings of the Royal Society B: Biological Sciences **281**, 20133280 (2014).

[4] R. Milo, S. Itzkovitz, N. Kashtan, R. Levitt, S. Shen-Orr, I. Ayzenshtat, M. Sheffer, and U. Alon, Superfamilies of evolved and designed networks, Science **303**, 1538 (2004).

[5] M. Huss and P. Holme, Currency and commodity metabolites: their identification and relation to the modularity of metabolic networks, IET Systems Biology **1**, 280 (2007).

[6] J. Kunegis, Konect (ACM, 2013) pp. 1343–1350.

[7] Y. Hu, A. Vinayagam, A. Nand, A. Comjean, V. Chung, T. Hao, S. E. Mohr, and N. Perrimon, Molecular interaction search tool (mist): an integrated resource for mining gene and protein interaction data, Nucleic Acids Research **46**, D567 (2018).

[8] M. D. Domenico, M. A. Porter, and A. Arenas, Muxviz: a tool for multilayer analysis and visualization of networks, Journal of Complex Networks **3**, 159 (2015).

[9] M. Ripeanu and I. Foster, Mapping the gnutella network: Macroscopic properties of large-scale peer-to-peer systems (2002).

[10] M. D. Domenico, A. Solé-Ribalta, S. Gómez, and A. Arenas, Navigability of interconnected networks under random failures, Proceedings of the National Academy of Sciences **111**, 8351 (2014).

[11] S. Knight, H. X. Nguyen, N. Falkner, R. Bowden, and M. Roughan, The internet topology zoo, IEEE Journal on Selected Areas in Communications **29**, 1765 (2011).

[12] J. Leskovec, D. Huttenlocher, and J. Kleinberg, Signed networks in social media (ACM, 2010) pp. 1361–1370.

[13] A. Paranjape, A. R. Benson, and J. Leskovec, Motifs in temporal networks (ACM, 2017) pp. 601–610.